https://doi.org/10.5194/egusphere-2025-4082
Preprint. Discussion started: 29 August 2025

Learning Evaporative Fraction with Memory

Wenli Zhao[1, 2, 3], Alexander J. Winkler[1, 3], Markus Reichstein[1, 3], Rene Orth[1, 4], Pierre Gentine[2]

[1] Max Planck Institute for Biogeochemistry, Jena, Germany.
[2] Columbia University, New York, USA.
[3] ELLIS Jena Unit, Jena, Germany.
[4] Faculty of Environment and Natural Resources, University of Freiburg, Germany.

Correspondence to: Wenli Zhao (dr.wenli.zhao.pku@gmail.com)

Abstract. Evaporative fraction (EF), defined as the ratio of latent heat flux to the sum of sensible and latent heat flux, is a key metric of surface energy partitioning and an indicator of plant water stress. Recognizing the role of vegetation memory effects, we developed an explainable machine learning (ML) model based on a Long Short-Term Memory (LSTM) architecture, which explicitly incorporates memory effects, to investigate the mechanisms underlying EF dynamics. The model was trained using data from 90 eddy-covariance sites across diverse plant functional types (PFTs), compiled from the ICOS, AmeriFlux, and FLUXNET2015 Tier 1 datasets. It accurately captures EF dynamics—particularly during post-rainfall pulses and soil moisture dry-down events—using only routinely available meteorological inputs (e.g., precipitation, radiation, air temperature, vapor pressure deficit) and static site attributes (e.g., PFT, soil properties). The ensemble mean predictions showed strong agreement with observations (R^2 = 0.82) across sites spanning broad climate and ecosystem gradients. Using explainable ML techniques, we identified precipitation and vapor pressure deficit as the primary drivers of EF in woody savanna, savanna, open shrubland, and grassland ecosystems, while air temperature emerged as the dominant factor in deciduous broadleaf, evergreen needleleaf, and mixed forests. Furthermore, expected gradients revealed variation in memory contributions across PFTs, with evergreen broadleaf forests and savannas exhibiting stronger influences from antecedent conditions compared to grasslands. These memory effects are strongly associated with rooting depth, soil water-holding capacity, and plant water use strategies, which collectively determine the time scales of drought response. Notably, the learned memory patterns could serve as proxies for inferring rooting depth and assessing plant water stress. Our findings underscore the critical role of meteorological memory effects in EF prediction and highlight their relevance for anticipating vegetation water stress under increasing drought frequency and intensity.

1 Introduction

Evaporative Fraction (EF), which represents the fraction of available energy used for evapotranspiration, is defined as the ratio of latent heat flux (LE) to the sum of LE and sensible heat flux (H): $\mathrm{EF} = \frac{\mathrm{LE}}{\mathrm{LE+H}}$ at the land surface. This ratio is critically linked to soil moisture (SM) availability, as it regulates evapotranspiration and therefore latent heat flux (Gentine et al., 2007; Nutini et al., 2014) and it also has a strong connection to vegetation greenness (Williams and Torn, 2015).

https://doi.org/10.5194/egusphere-2025-4082
Preprint. Discussion started: 29 August 2025

Previous studies have shown that EF is mainly governed by root zone water availability and vegetation structure and is intrinsically linked to precipitation-supplied water resources (Bastiaanssen et al., 1997; Gentine et al., 2007; Ichii et al., 2009). As a result, EF can offer valuable insights into plant water status, and water stress, and their survival strategies during water stress conditions. A slowly declining EF during periods of droughts is indicative of a deep root system, which ensures sustained access to deep water stores (Dralle et al., 2020; Stocker et al., 2023) (Figure 1).

Current studies indicate that vegetation exhibits both resilience and resistance, collectively referred to as memory effects, during different ecosystem processes, particularly after climate extremes (He et al., 2018; Hossain et al., 2022; Canarini et al., 2021). Vegetation dynamics are shaped not only by the concurrent climate conditions but also by lagged- or memory-induced responses. For instance, favourable climate in the past may trigger vegetation overgrowth beyond the ecosystem's carrying capacity, increasing vulnerability to subsequent stress events (Zhang et al., 2021). Temperature anomalies, including heat and cold stresses, can impair vegetation function, alter its water demand (via temperature-induced soil moisture memory) and deplete carbon reserves, which in turn influence transpiration and daily EF variability (Staacke et al., 2025). Memory effects thus reflect both the capacity of ecosystem to return to equilibrium after disturbances (Xiao et al., 2024) and their ability to maintain functional stability under ongoing stress (Hossain et al., 2022; Yu et al., 2021). In Figure 1, we highlight how rooting depth, a key plant trait, mediates these memory responses to climate extremes (e.g., droughts). Despite previous efforts to explore EF mechanisms, direct observational evidence that explicitly incorporates memory effects remains limited, calling for robust analytical tools to capture and interpret the memory effect from the complex interactions between drivers.

Recent advances in machine learning (ML) algorithms have shown promise in capturing complex hydrological processes, including surface fluxes, snowpack or streamflow prediction with the effect of lagged response (ElGhawi et al., 2023; Feng et al., 2020; Jiang et al., 2022a; Pan et al., 2020; Reichstein et al., 2019, 2022; Zenone et al., 2022). However, few studies have explicitly embedded memory effect in EF predictions. Long Short-Term Memory (LSTM) networks – a variant of recurrent neural networks, are particularly well suited for learning from sequential data and are increasingly used to model temporal dynamics in hydrology (Fang and Shen, 2020; Jiang et al., 2020; Li et al., 2022). LSTM, with its recurrent cells, retains previous information from input sequences akin to how meteorological data, like precipitation, and its impact is retained over long periods of time as soil moisture or snowpack (Lees et al., 2021, 2022). In the context of vegetation, previous heat stress events can cause cellular damage that impairs photosynthesis, respiration and transpiration, ultimately altering EF (Staacke et al., 2025). The hidden states in LSTM encode system memory and evolve with time, interacting with real-time climate variables to simulate time series (Xiao et al., 2024). This allows the model to account for historical vegetation-climate interactions in a data-driven way - without relying on process-based models that often misrepresent such memory effect (Kraft et al., 2022; Lees et al., 2022). Instead, it infers such information through the memory effects captured within its recurrent cells, learning functional dependencies between EF and both current and past climate drivers such as precipitation and temperature anomalies.

https://doi.org/10.5194/egusphere-2025-4082
Preprint. Discussion started: 29 August 2025

Combined with feature attribution techniques (i.e., Expected Gradients), our proposed explainable ML framework could then extract the captured patterns and interpret the memory from "black-box" ML models. Such tools have recently led to theoretical breakthroughs in climate, ocean, and weather sciences (e.g., Tom et al., 2020; Barnes et al., 2020; Labe and Barnes, 2021), including the identifying flooding drivers (Jiang et al., 2022). In our context, interpretability enables understanding of EF's memory-driven behaviours, tracking plant water stress, and even potentially inferring rooting depth (Collins and Bras, 2007; Fu et al., 2022; Liu et al., 2020; Wang et al., 2006). The identification of memory effect would not only enhance our process-based understanding of EF mechanisms, but also enable EF to serve as a more objective indicator of plant stress - one that operates independently of soil moisture estimates and is directly linked to surface evapotranspiration processes, with memory effects related to plant regulation embedded within the algorithms (Kraft et al., 2019).

In this study, we employ explainable ML to explore the memory dynamics of EF using long-term observations from 90 eddy covariance (EC) sites (>5 years) across ICOS, AmeriFlux, and FLUXNET2015 Tier 1 dataset, combined with remote sensing data. Our framework is designed to:

1. Capture complex functional relationships between climate drivers and EF across diverse plant functional types (PFT), incorporating memory effects;
2. Apply expected gradients to identify key drivers of EF predictions across different PFTs and disentangle their memory effect contributions at the event-level.
3. Investigate how memory effects vary across diverse PFTs and relate to key site characteristics such as rooting depth, soil water holding capacity (i.e., the soil matric suction) and aridity index.

Overall, this study advances understanding of EF regulation and memory effect. It demonstrates how explainable ML can uncover plant water-use strategies under diverse environmental regimes.

https://doi.org/10.5194/egusphere-2025-4082
Preprint. Discussion started: 29 August 2025

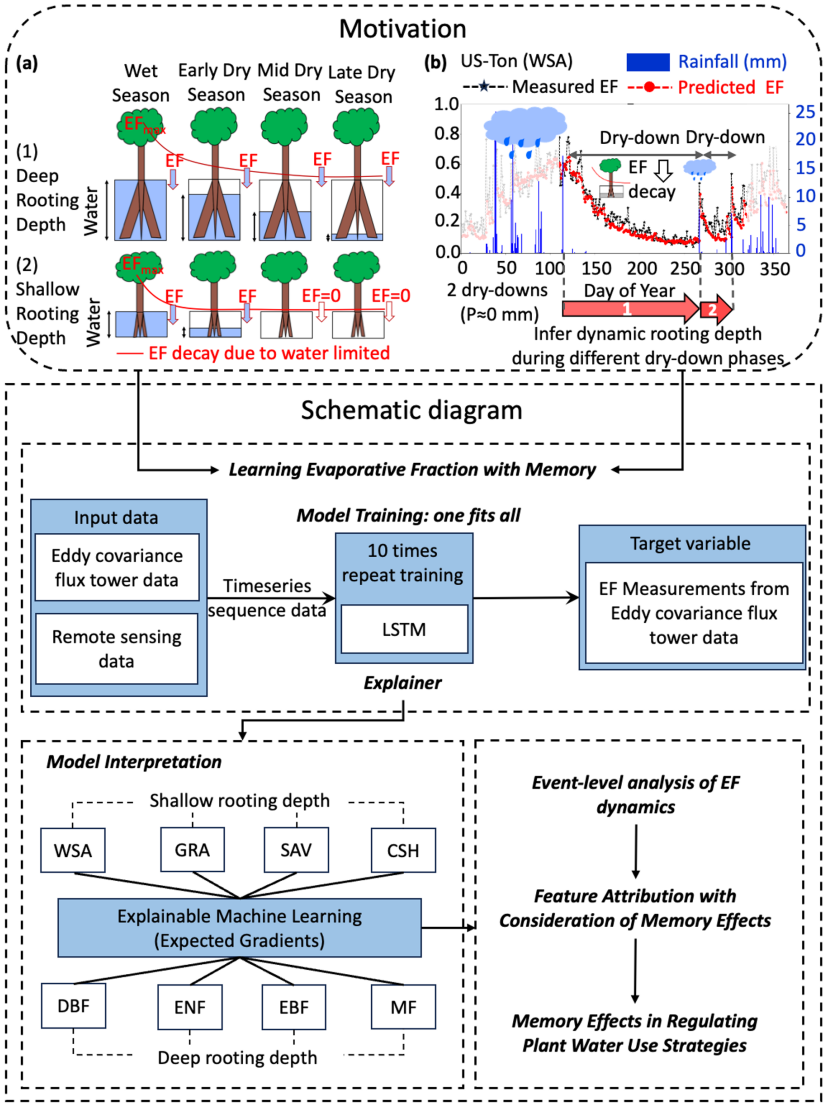

Figure 1. The motivation and schematic diagram of this study. Upper Panel: The motivation plot of this study. (a) indicates a water bucket model showing the EF decay during the dry downs. In the wet season, the precipitation fills up the vegetation water bucket and EF peaks. Then during the dry season, the vegetation will consume the available water storage during the wet season and thus EF decay could be observed. If the vegetation has a deep rooting depth, the EF decay will tend to be slow during the dry season. If the vegetation has a shallow rooting depth, the EF decay will tend to be fast during the dry season due to less available water storage compared to the deep rooting depth vegetation. Adapted from the Figure 3 in Ichii et al., 2009. (b) indicates a field experiment on a woody savanna site (US-Ton). The observations support our hypothesis in plot (a). Precipitation provides the available water storage and EF peaks, then there's a EF decay during the dry downs. The rooting depth information is hidden in the slow and fast EF dry downs. If we could predict EF accurately, we could potentially infer dynamic rooting depth and use EF as a direct water stress index. Lower Panel: The schematic diagram of this study. A long short-term model (LSTM) with memory effect is used here to capture the schemes expressed in the upper panel. The model is trained using eddy covariance flux tower data and remote sensing data. We train a general model for all the sites and then use explainable machine learning technique to analyze the drivers for each plant functional types and sites. Further investigations have been conducted to explore the relationship between memory effects and rooting depth, soil water holding capacity and aridity index across various PFTs.

https://doi.org/10.5194/egusphere-2025-4082
Preprint. Discussion started: 29 August 2025

2 Data Collection and Preprocessing

2.1 Eddy covariance measurements

We used 215 eddy-covariance sites from the combined ICOS (https://doi.org/10.18160/2G60-ZHAK), AmeriFlux (https://ameriflux.lbl.gov/data/download-data/), FLUXNET 2015 tier 1 dataset (https://fluxnet.org/data/fluxnet2015-dataset/), covering 11 Plant Functional Types (PFTs) according to the IGBP (International Geosphere-Biosphere Programme) vegetation classification scheme (Loveland et al., 2000), including evergreen needleleaf forests (ENF), evergreen broadleaf forests (EBF), deciduous broadleaf forests (DBF), deciduous needleleaf forests (DNF), croplands (CRO), grasslands (GRA), savannas (SAV), woody savannas (WSA), closed shrublands (CSH), and mixed forests (MF), open shrub (OSH). The map of the site distributions is shown in Figure S1. Data for all the sites can be accessed via the links provided in Table S1. We first exclude the sites without latent heat flux, sensible heat flux, surface shortwave incoming radiation, precipitation, vapor pressure deficit (VPD), air temperature, wind speed measurements from the analysis; then we drop all cropland and wetland sites, as cropland sites are usually affected by management practices such as irrigation, and wetland sites usually have a perched water table. Next, we only kept the sites which has more than 5 years of observations after we applied the data preprocessing steps (further aggregated from half-hourly to daily scale), detailed in the following paragraph and supplementary materials (Text S1). These preprocessing steps help to reduce the data imbalance issue in parameter optimizations during the training of the models. The final dataset consists of 90 sites.

2.2 Evaporative Fraction Calculations

The Evaporative Fraction was calculated using the formula EF = LE/(H+LE), where LE represents the corrected latent heat flux and H the corrected sensible heat flux. We assume the errors in LE and H exhibit comparable magnitudes, as suggested by previous studies (Foken, 2008; Hollinger and Richardson, 2005; Richardson et al., 2006), and are uncorrelated. This assumption enables to mathematically eliminate the errors associated with the lack of energy balance closure (Schwalm et al., 2010).

2.3 Auxiliary Datasets

The leaf area index (LAI) data is obtained from the simultaneous MODIS product MCD15A3H using the Global Subset Tool (https://modis.ornl.gov/globalsubset/). The temporal resolution is 4 days. LAI does not significantly change within 4 days, so we used this LAI value as the daily input of our algorithms. The soil attribute data is from SoilGrid with a resolution of 250 meters, including clay, silt and sand content (Poggio et al., 2021).

Root depth information is obtained from the global rooting depth dataset compiled by Stocker et al. (2023), and the long-term evapotranspiration (ET) data used for dryness and wetness classifications are extracted from the TerraClimate dataset via Google Earth Engine (Abatzoglou et al., 2018).

https://doi.org/10.5194/egusphere-2025-4082
Preprint. Discussion started: 29 August 2025

3 Methodology

3.1 Long Short-Term Memory Model

A machine learning model using the Long Short-Term Memory architecture, which explicitly accounts for memory effects, is used to predict the daily scale EF. We test different combinations of hyperparameters, including the number of LSTM layers and neurons per layer, to determine the most appropriate model structure (Figure S2, S3). The finalized model structure consists of 3 layers with activation functions as follows: one LSTM layer with 128 neurons, fully connected dense layer with 36 neurons and one output dense layer with 1 neuron.

We choose dynamic variables including daily sum precipitation (P), daily mean wind speed (WS), daily mean surface shortwave incoming radiation (RAD), daily mean air temperature (Ta), daily mean VPD, LAI and site-specific static variables including soil properties and PFTs as the input features. In addition, annual mean P, annual mean RAD, annual mean Ta are also input of the model to account for climatic differences.

3.2 Baseline model

To benchmark the predictive capacity of LSTM model, we choose three baseline approaches for comparisons: 1) a fully connected neural network (NN) as a baseline for EF prediction. Like the process of defining the LSTM model structure, we tested different combinations of hyperparameters, including the number of fully connected layers and neurons per layer, while ensuring a fair comparison with the LSTM model. The final fully connected neural network model structure is as follows: it consists of two fully connected dense layer with 128 neurons, one fully connected dense layer with 36 neurons and one output dense layer with 1 neuron (Figure S2, S3). The length of time series sequence data is same with the input for the LSTM model, 2) an EF climatology model. We calculate the climatology of EF as the baseline to show the LSTM's capacity in capturing the EF dynamics after the rain-pulse events. 3) a Standardized Precipitation Index (SPI)-based fitting model.

$EF = \beta_0 \times \tan(\beta_1 \times SPI + \beta_2)$, where β_0, β_1, and β_2 are three regression model parameters.

3.3 Training/Validation/Test Set Setups

The datasets were partitioned by time, with one year from each site randomly selected for testing and validation, while the remaining site-years were used for training. Notably, we also experimented with a site-based split, which yielded slightly lower model performance (R^2 = 0.72; see Figure S4) compared to the time-based strategy. However, since our primary objective is to use LSTM to investigate EF dynamics and memory effects, we opted for the time-based split to ensure a more representative and interpretable explainer model.

Then we set up 10 models only varying in the initialization of the weights and biases of LSTM and NN and train each model with different memory lengths to reduce the randomness and obtain a measure of uncertainty. The memory length varies from 10 to 360 days with 30-day intervals (365 days is also added to test) to identify the most appropriate memory length

https://doi.org/10.5194/egusphere-2025-4082
Preprint. Discussion started: 29 August 2025

that yields the best prediction skill (Figure S3). Early stopping is used to avoid overfitting and find the best model for prediction.

After 10 times' repeat training for each memory length, we also calculate the ensemble mean predictions (average value of the 10 models' predictions) as the robust EF prediction.

3.3 Soil moisture drydown identification

Drydowns following rainfall are defined as periods with no precipitation for several consecutive days, during which soil moisture exhibits a short-term 'pulse' increase after a rain event, followed by a gradual decline until the next rainfall. At each flux tower site, we retained drydown events for analysis if soil moisture decreased continuously for at least 7 days after rainfall, following the criteria used in previous studies (Fu et al., 2024; McColl et al., 2017). We also tested more stringent thresholds of 9 and 11 days for the minimum drydown duration, and found that the results remained consistent.

3.4 Model Interpretations – Expected Gradients (EG)

Considering the potential collinearities among the predictors and the aim to attribute contributions to each time step, we implemented the expected gradients techniques to further exploit the feature importance at each time step, revealing the specific contributions of inputs to daily EF predictions (see details in Text S2). Compared to permutation feature importance, this approach enables our temporal model to break down the overall importance of features into specific contributions at each time step (Jiang et al., 2022b; Molnar, 2019). This detailed analysis allows us to examine the response of plants across varying memory effects under extreme events or environmental conditions – a capability not present in non-temporal models.

4 Results and Discussions

4.1 Model Performance Across All Plant Functional Types of LSTM with benchmark models

Figure 2 presents the efficacy of our trained LSTM models with the memory length setting with 365 days. We repeated the training process for 10 times while sampling different initial parameters of the ML models. This approach mitigates the randomness inherent in the ML model parameter optimization and provides a quantification of uncertainty. The whole datasets were separated by time, with one year from each site randomly selected for testing and validation, and the remaining site-years used for training (Methods). The results suggest that overall, the LSTM models achieved good accuracy in EF prediction, compared to the EF observations of EC towers for test set (at site-years never seen by the model during the training and validation process). The model achieved a high predictive accuracy, with a mean R^2 of 0.81 across 10 repeated runs using a memory length of 365 days, when compared against observations from EC sites. Employing ensemble means of multiple machine learning models is a well-established strategy for enhancing generalization and mitigating overfitting, particularly in complex, nonlinear systems (Dietterich, 2000). This approach has been successfully adopted in recent

https://doi.org/10.5194/egusphere-2025-4082
Preprint. Discussion started: 29 August 2025

studies—including those in Earth system modeling contexts (e.g., Kraft et al., 2019; Jung et al., 2019; Jiang et al., 2022; Nelson et al., 2024). The improved performance of the ensemble mean highlights its ability to capture complex nonlinear interactions and memory effects from high-dimensional input features—patterns that are often challenging for traditional process-based models to reproduce. We therefore recommend using an ensemble approach for both final prediction and model interpretation.

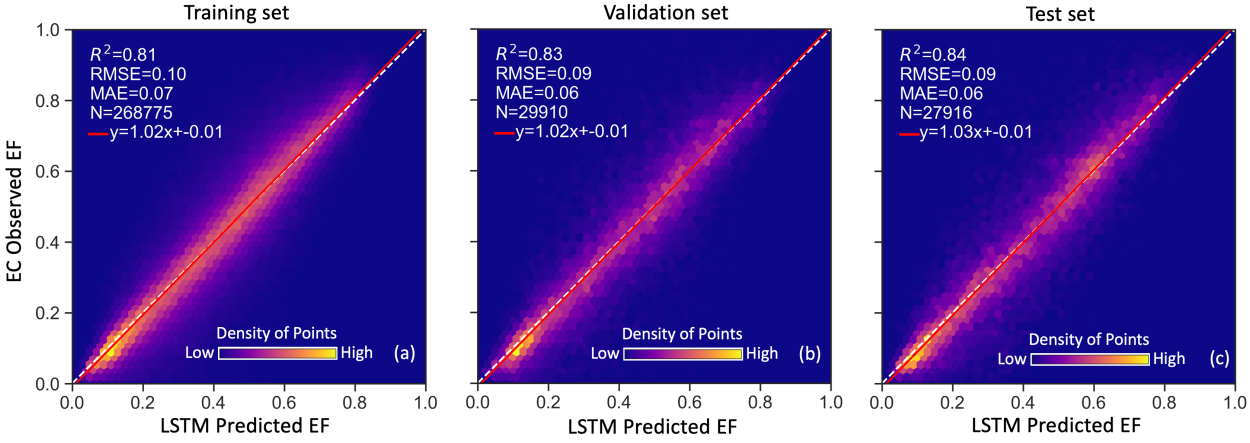

Figure 2. Model performance across the sites in training, validation and test set. (a), (b) and (c) indicate the model performance with 365 days' time series data as input for training, validation and test set, respectively. The EF predictions shown here are based on the ensemble mean EF predictions of 10 repeated models. The density of scatter points is represented using shading colors. The diagonal black dashed line depicts the 1:1 line and the red solid line depicts the linear regression line. Note that N, R^2, and RMSE represent the number of points, coefficient of determination, and root mean square error, respectively.

We further evaluated model performance at both the site and PFT levels across all periods, as well as during drydown and non-drydown periods, to assess whether the LSTM specifically captures EF dynamics beyond simply learning climatology or serving as a proxy for soil moisture. The results demonstrate that the LSTM consistently outperforms the baseline models in all scenarios. The average site-level R^2 for the LSTM is 0.68, calculated by first determining the R^2 between predicted and observed EF at each site, then averaging across all sites. In comparison, the baseline models yield lower mean R^2 values: 0.55 for FNN, 0.47 for the climatology-based model, and 0.04 for the SPI-based model. Notably, the baseline models perform poorly during post-rain pulse drydown periods, with average R^2 values dropping to 0.36 (FNN), 0.12 (CLIM), and –1.21 (SPI-based). Even during non-drydown periods, their performance remains suboptimal, with R^2 values of 0.51 (FNN), 0.44 (CLIM), and 0.03 (SPI-based). In contrast, the LSTM model maintains relative good predictive skill in both conditions, achieving an R^2 of 0.54 during drydowns and 0.65 during non-drydown periods. These findings highlight the LSTM's strength as an explanatory model for EF dynamics, capable of capturing both short-term post-rain responses and background variability beyond what simpler models can achieve (Figure 4).

This underscores the importance of the memory effect and the superiority of the LSTM architecture in accurately predicting EF. The LSTM model, comprising input, forget, and output gates, manages to long-range retain or discard patterns in

https://doi.org/10.5194/egusphere-2025-4082
Preprint. Discussion started: 29 August 2025

meteorological data, thereby capturing long-term dependencies effectively. Crucially, this mechanism is analogous to a water infiltration and retention in the soil and slow evapotranspiration processes, where prior rainfall is conserved as soil moisture and later accessed by plants' root systems for plant function and growth (Dralle et al., 2020). Consequently, our model can accurately simulate the physical process of plant water usage during dry spells and its time dependence as sketched in Figure 1.

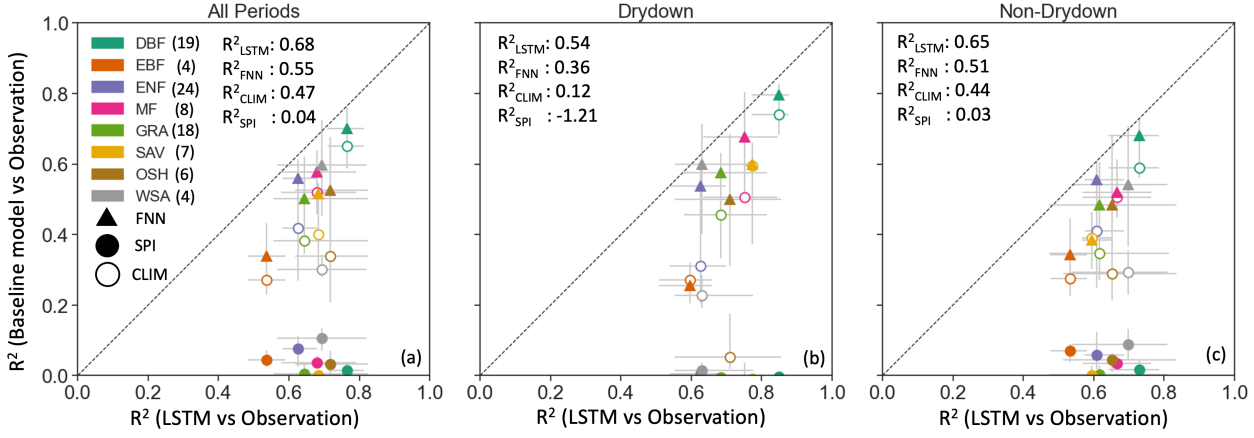

Figure 3. Comparison of model performance between the LSTM and baseline models. (a) Model performance across all periods. (b) Performance during drydown events. (c) Performance during non-drydown periods. Each point represents the mean site-level R^2 between predicted and observed EF, computed using the general LSTM model (X-axis), and compared against baseline models (Y-axis), including FNN (triangle), SPI-based (solid circle), and CLIM (open circle). Site-level R^2 values were first calculated individually and then averaged across all sites. Points falling below the 1:1 dashed line indicate that the LSTM outperforms the corresponding baseline model. Error bars represent the interquartile range (25th to 75th percentiles). R^2 denotes the coefficient of determination between predicted and observed evaporative fraction. Site counts are shown in parentheses.

https://doi.org/10.5194/egusphere-2025-4082
Preprint. Discussion started: 29 August 2025

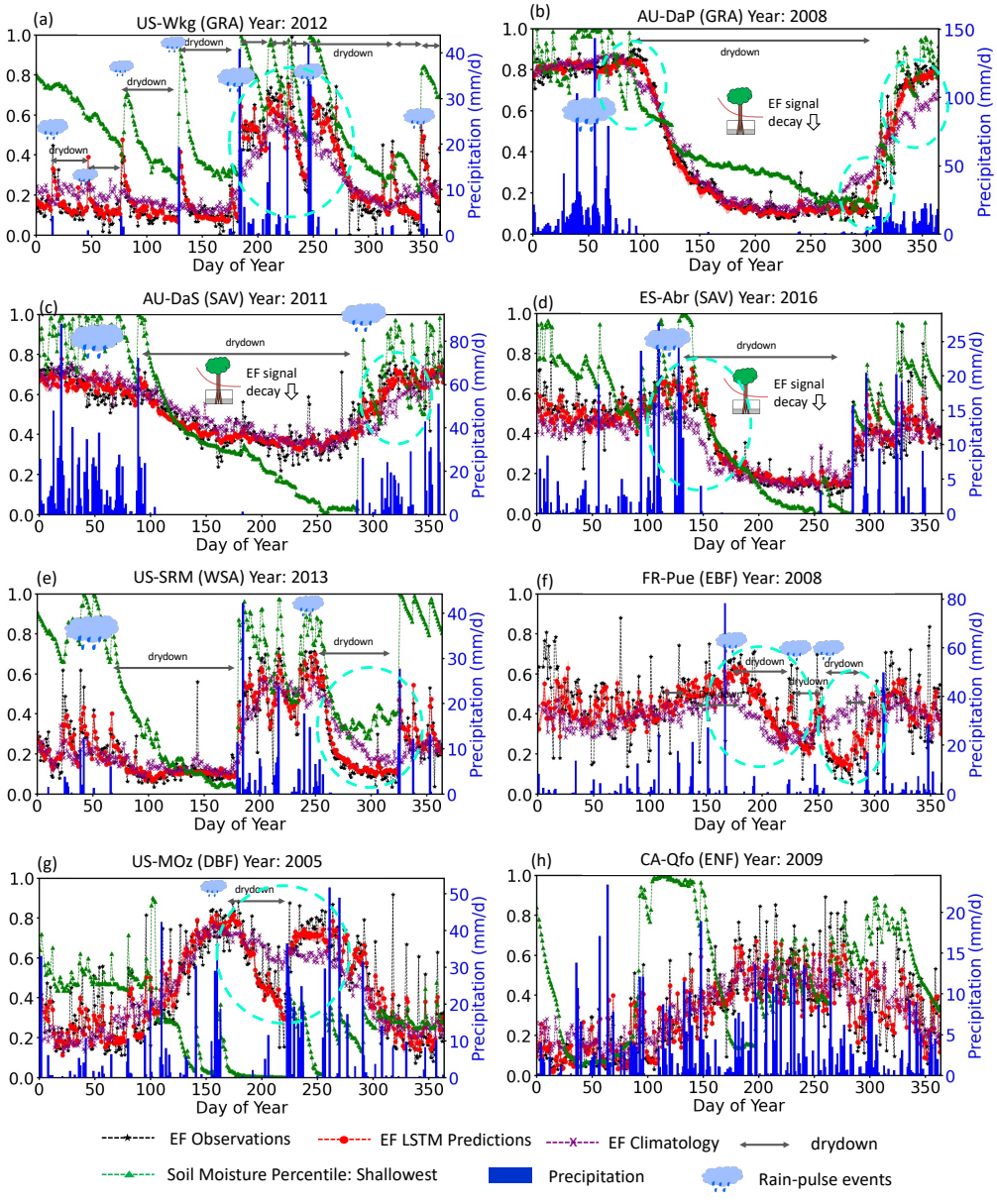

Figure 4. Prediction of Evaporative Fraction Dynamics Across Various Plant Functional Types. Daily time series of Evaporative Fraction (EF) dynamics for several cases of dry-down periods, as estimated by machine learning models considering memory effects. Blue bars show the observed daily sum precipitation (P), black curves show EF observations, red curves show EF predictions, green curves show soil moisture percentiles of the shallowest soil depth. The x-axis represents the day of year (DOY) of the whole year. Labels in the panels show the auxiliary information of the detected dry-down periods (GRA: grassland, WSA: woody savanna, SAV: savanna, DBF: deciduous broadleaf forest, ENF: evergreen needleleaf forest). The daily volumetric water content values are converted into percentiles, indicating the fraction of daily values lower than a specific value. Thus, the 100th percentile (or a percentile value of 1) represents the wettest soil conditions observed at a specific site throughout the study period, and the 0 percentile signifies the driest soil conditions. The length of time sequence input is set as 365 days for the machine learning model. The EF predictions here are using the ensemble mean EF predictions of 10 models with different initializations. Shaded areas represent regions of predictions uncertainty in the 25%-75% quartiles of these 10 repeat training models. Note all the results shown here are from the test set.

https://doi.org/10.5194/egusphere-2025-4082
Preprint. Discussion started: 29 August 2025

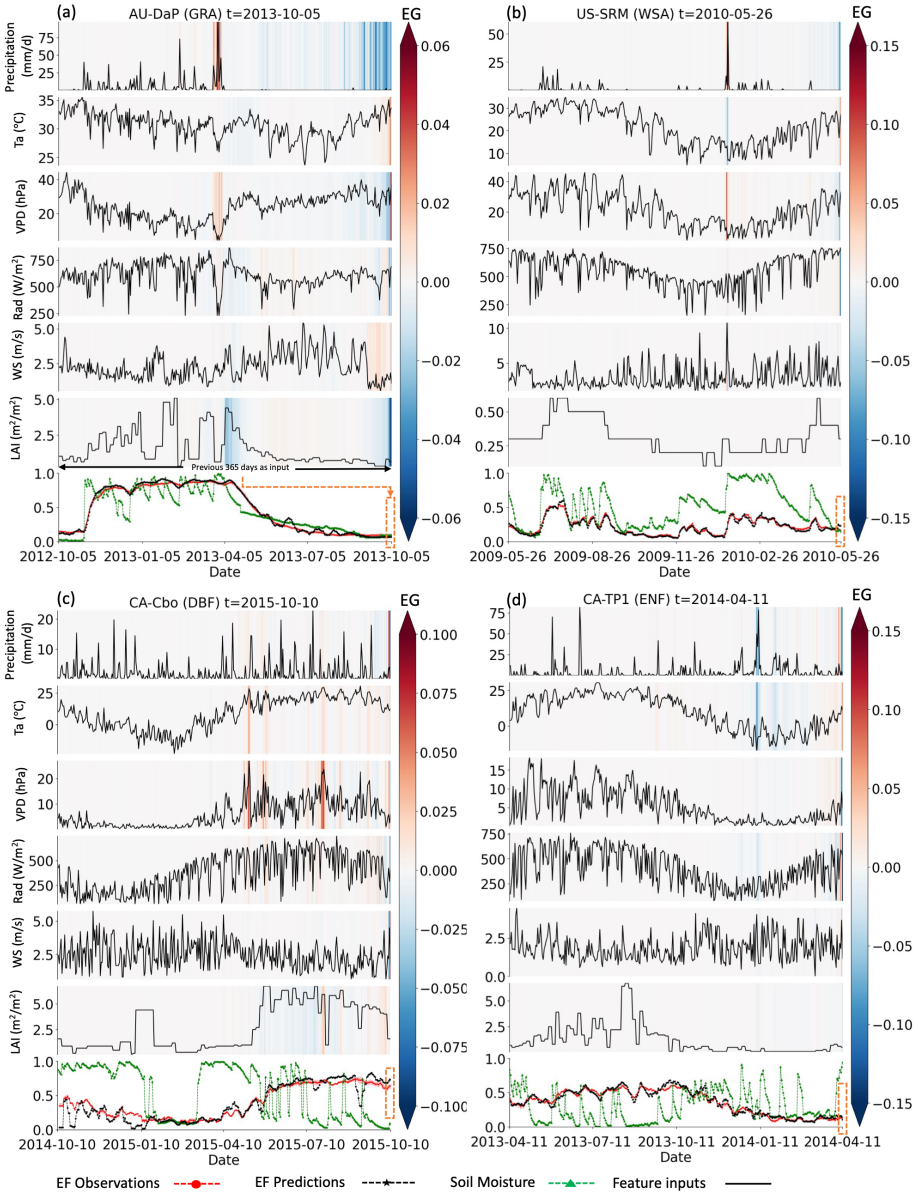

Figure 5. Examples of memory effects revealed by expected gradients. (a) A grassland site (AU-DaP, 2013-10-05). The LSTM model uses the previous 365 days of input data (from 2012-10-05 to 2013-10-15) to predict EF on 2013-10-05. The expected gradients illustrate the influence of antecedent climate variables—precipitation, air temperature, vapor pressure deficit (VPD), and net radiation—on the current EF prediction. In this long drydown event, precipitation around 2013-04-05 shows a positive contribution to EF, which is plausible as it replenishes soil water storage for the subsequent dry period. Notably, VPD and LAI also exhibit significant influence, suggesting that prior atmospheric dryness and vegetation status modulate how stored water is used, ultimately shaping EF behavior during the drydown. (b) A woody savanna site (US-SRM, 2010-05-06); (c) a deciduous broadleaf forest site (CA-Cbo, 2015-10-10); and (d) An evergreen needleleaf forest site (CA-TP1, 2014-04-11), where an extremely low-temperature event around 2014-01-11 appears to affect EF predictions approximately three months later. This delayed influence may reflect the impact of cold stress on vegetation functioning,

https://doi.org/10.5194/egusphere-2025-4082
Preprint. Discussion started: 29 August 2025

potentially reducing transpiration capacity and altering EF. Expected gradient patterns across all sites are summarized in the subsequent figures.

The contribution of each individual time step indicated by the Expected Gradients (see Methods) clearly shows the impact of previous rainfall on the current EF predictions (Figure 5(a)(b)(c)). This reflects the positive impact of previous precipitation (lag effect), especially closest to the prediction time, and negative impact of dry spells to EF predictions (Figure 5a). Additionally, past episodes of extremely low temperature may also suppress vegetation functioning, as reflected in EF predictions during April at the CA-TP1 site (Figure 5d). These examples demonstrate that the LSTM effectively learns the influence of both climate variability and extreme events on EF dynamics, including their temporal lag effects. We summarize all the explainable EGs for all the sites in the following figures (Section 4.3).

4.2 Reconstruction of Evaporative Fraction Dynamics During Soil Moisture Dry-Down Periods

Our model adeptly captures the observed EF dynamics as observed in the unseen site-years, particularly during soil moisture dry-down periods across grassland, savanna and woody savanna sites, as illustrated in Figure 4. The decay in EF predictions aligns with the observed decline in shallow soil moisture, corroborating soil water processes where wet season precipitation supplies the initial water for prolonged dry periods which is then slowly decaying through evapotranspiration (only shallow soil moisture observations are used here for comparisons due to the data limitation). Consequently, EF peaks, and then gradually decreases at varying rates during drydown intervals, with a pace reflecting diverse evaporative demand and vegetation rooting depths and plant water usage strategies. For example, grasslands, with typically shallow roots, exhibit a faster EF decay compared to savannas, which suggest a deeper rooting system and/or lower canopy conductance for the latter (Figure 4), consistent with in-situ observations (Dralle et al., 2020; Fan et al., 2017; Ichii et al., 2009; Seyfried and Wilcox, 2006). However, we also note the diversity of climatic environments in which the different grassland sites are situated. For instance, AU-DaP experiences sufficient precipitation only in certain seasons, whereas precipitation at AT-Neu is more evenly distributed throughout the entire year (Figure S5). Some grassland sites receive sufficient rainfall during the whole years like the deciduous broadleaf and evergreen broadleaf forest sites. This leads to differences in the characteristics of their EF drydowns. The investigations of the variations in EF decay rates offers a promising avenue for inferring rooting depths, and plant water-use strategies across sites and underscores EF's potential as an indicator of vegetation-regulated water stress responses. In contrast to the sporadic rainfall patterns typical of grasslands and savannas, deciduous broadleaf forest and evergreen broadleaf forest sites experience abundant precipitation throughout the year. This consistent moisture supply contributes to substantial variability in observed EF, likely due to processes such as canopy interception (Lian et al., 2022). The differing rates of soil moisture dry-down among these sites likely reflect variation in plant rooting depths and water use strategies, which in turn influence the characteristic time scales of drought response. These findings also

https://doi.org/10.5194/egusphere-2025-4082
Preprint. Discussion started: 29 August 2025

underscore the importance of incorporating memory effects when analyzing EF dynamics across different plant functional types and site-specific conditions.

4.3 Drivers of EF Dynamics Incorporating Memory Effects

Delving into the causes of rapid and gradual EF decreases, we analyze the trained EF model using explainable machine learning techniques, namely expected gradients (Erion et al., 2021; Molnar, 2019; Sundararajan et al., 2017). EG is a method for attributing the prediction of a neural network to its input features by integrating gradients along the path from randomly sampled baselines to the actual input and averaging over these attributions. This analysis not only revealed the controlling factors in predicting EF but also delineated the temporal influences, allowing us to ascertain the general feature importance alongside the distinct contributions to each individual time step. Consequently, the feature importance obtained through EGs inherently includes the memory contributions from historical periods for each variable, thus potentially considering the memory effect and the legacy effect.

First, we summarize the EGs by calculating the relative contribution for each variable (in %). This is achieved by dividing the total sum of absolute EGs for each variable. For all the sites put together, the absolute EGs identified precipitation (25%) and air temperature (22%) as the most two influential drivers. This is followed by radiation (21%), vapor pressure deficit (18%), wind speed (7%), and leaf area index (6%). Precipitation feeds the available water resources, i.e., root-zone soil layer, used to sustain the ecosystem during droughts. Air temperature and precipitation emerged as more dominant than radiation when memory effects are considered. Although radiation is a key driver of instantaneous evaporative demand through energy input, the LSTM model's ability to account for memory and legacy effects likely explains the elevated importance of temperature. This suggests that while radiation influences short-term EF variation, air temperature plays a more critical role over longer timescales, highlighting the necessity of incorporating memory effects when predicting EF and related land-atmosphere fluxes. VPD provides a measure of atmospheric aridity, significantly affecting ET and thus EF. LAI did not emerge as a dominant feature for EF prediction, partly due to spatial and temporal discrepancies in the MODIS LAI product (250 meters, 4-day) but also to the fact that most variability in EF at dry sites is due to soil moisture decay and driven by (lack of) precipitation. Cloud cover or aerosols may also contaminate the MODIS LAI data (Yang et al., 2006). Wind speed's minimal effect on EF predictions aligns with recent data-driven research (Gentine et al., 2011; Lhomme and Elguero, 1999; Zhao et al., 2019), showing that evapotranspiration is not strongly affected by wind speed. However, we also note that the significance of input features importance varies among different sites, different PFTs and climatic regions (Figure 6, Figure 7). In general, the water controls, i.e., precipitation, VPD are the two main drivers for most of woody savanna, savanna, open shrubland and grassland sites, whereas air temperature emerges as the dominant factor for most forest sites for deciduous broadleaf forest, evergreen needleleaf forest and mixed forest sites (Figure 7), which is consistent with previous studies(Chen et al., 2018; Guérin et al., 2020).

https://doi.org/10.5194/egusphere-2025-4082
Preprint. Discussion started: 29 August 2025

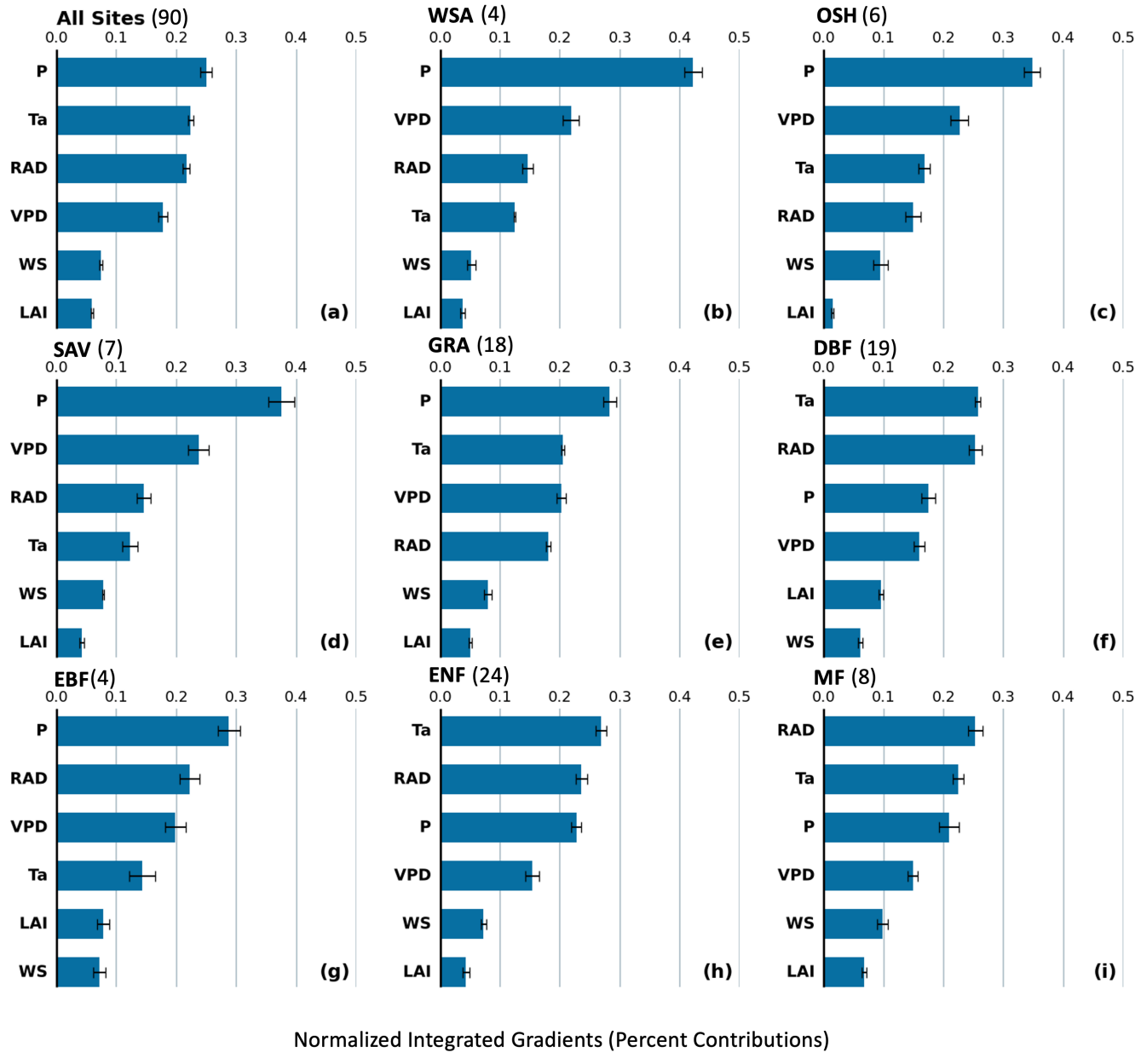

Figure 6. Feature Importance Revealed by the Temporal Evaporative Fractions Model Considering the Memory Effect. a indicates the overall feature importance across all the plant functional types. b, c, d, e, f, g, h, i represents the feature importance for woody savanna (WSA), open shrubland (OSH), savanna grassland (SAV), deciduous broadleaf forest (DBF), evergreen broadleaf forest (EBF), evergreen needleleaf forest (ENF), mixed forest (MF). Note that the EG values are normalized by percent contributions, that is, divided by the total sum of absolute EGs for all the variables shown here in each plot. Thus the values here indicate a relative percent contribution (e.g., 0.3 means 30%). Site counts are shown in parentheses.

https://doi.org/10.5194/egusphere-2025-4082
Preprint. Discussion started: 29 August 2025

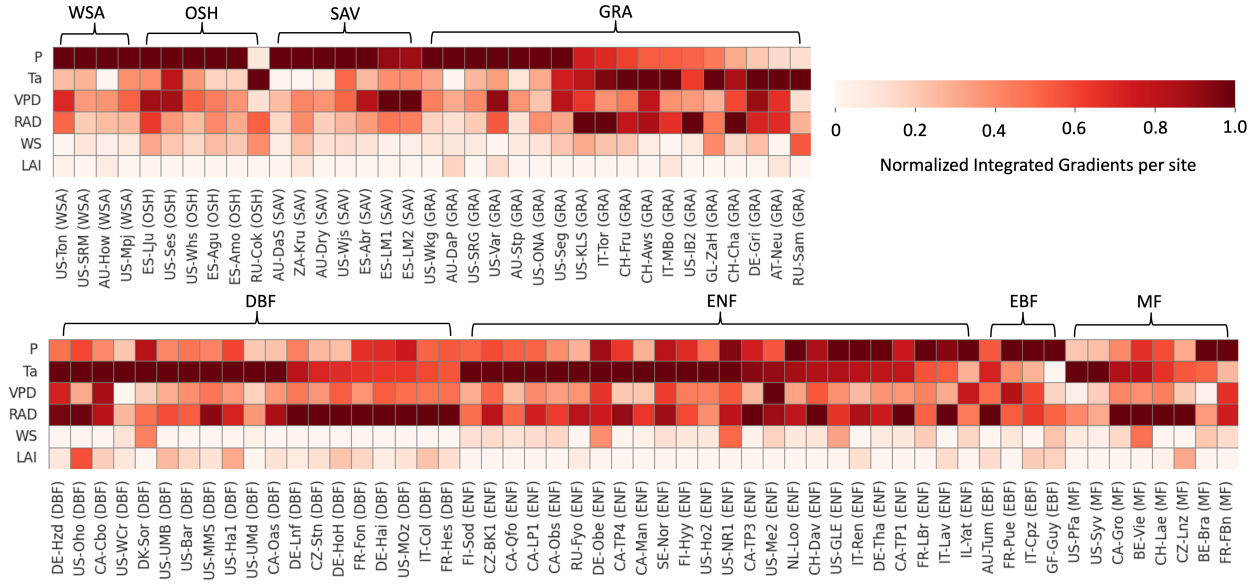

Figure 7. Feature Importance Revealed by the Temporal Evaporative Fractions Model Considering the Memory Effect for each site. Note that the absolute EG values are normalized by using minimum and maximum EG values in each site. Thus, the values here with 1 most important, while 0 least important to the evaporative fraction predictions.

Recent studies have also highlighted temperature-related memory—often referred to as heat stress (HS) memory—at the molecular scale, revealing mechanisms and regulatory layers involved in HS memory formation and resetting. These processes play a crucial role in enhancing plant stress resilience and fitness. During episodes of excessively high temperatures, plants can suffer cellular damage, primarily due to impaired photosynthesis and respiration, accumulation of misfolded proteins, and the production of reactive oxygen species. In natural environments, plants frequently encounter multiple recurring heat stress events rather than isolated incidents. The timing of these events can vary considerably, with subsequent extremes occurring shortly after or long after the initial one (Staacke et al., 2025). This variability can significantly influence vegetation functioning and transpiration—and thereby, evaporative fraction—at later stages. Moreover, the lag time of vegetation response to high temperatures is generally longer in mid- and high-latitude regions than in low-latitude ecosystems (Xiao et al., 2024). Forests, for instance, tend to initiate resistance mechanisms earlier due to their deeper rooting systems. However, once physiological functions are affected, forests are slower to recover (Xiao et al., 2024). In contrast, grasslands, though often more vulnerable to climate extremes, typically recover more quickly (Ying et al., 2020). Overall, the differences in rooting depth and water-use strategies across vegetation types may create a trade-off between resistance and resilience, potentially leading to post-extreme spatial heterogeneity in vegetation responses. This underscores the importance of further investigating how such memory effects—especially temperature-induced—manifest across ecosystems and influence EF.

https://doi.org/10.5194/egusphere-2025-4082
Preprint. Discussion started: 29 August 2025

4.4 Memory Effects: Uncovering Hidden Mechanisms in Plant Water Use Strategies

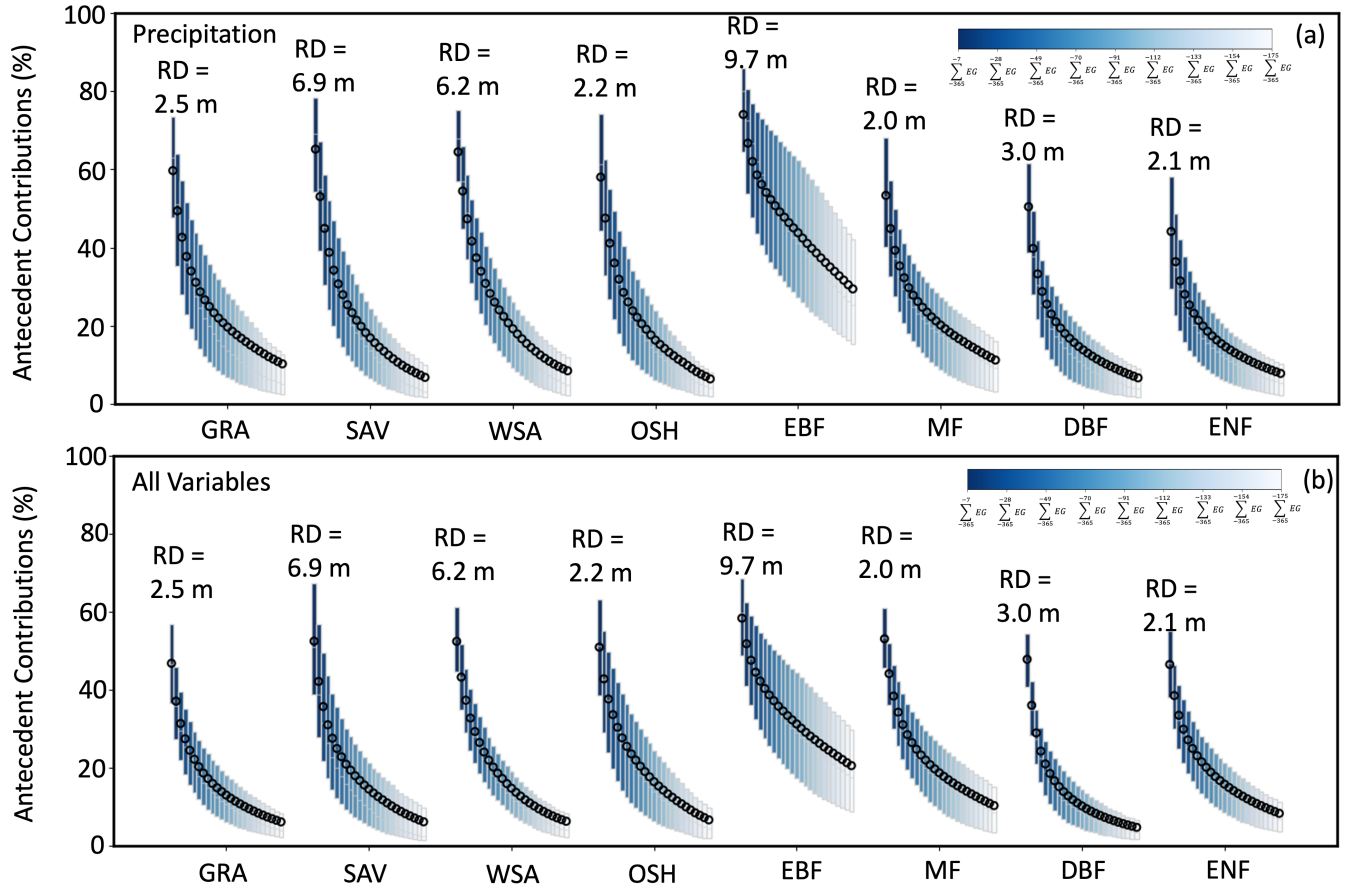

Figure 8. Memory Effect Contributions of Preciptation and Total Variables in Predicting Evaporative Fraction. The sum of expected gradients (EG) for different antecedent periods, e.g., $\sum_{-365}^{-7} \boldsymbol{EG}$ represents the sum of absolute EGs between previous 7 and 365 days, for precipitation (a), All Variables (b). The sum absolute EGs are further normalized to a relative percent contribution for easy comparison.

Our temporal EF model, unlike non-temporal models in previous studies, distinguishes general feature influenced at individual time steps through integrated gradient values, shedding light on the temporal mechanics of EF. We then further summarize the EGs by different time steps, e.g., $\sum_{-365}^{-7} EG$ represents the sum of absolute EGs ranging from the previous 7 to 365 days, for different drivers (Methods). The sum absolute EGs are further normalized to a relative percent contribution for easy comparison. The memory effect here is indicated by the relative contributions (in %) of the antecedent time steps in each variable. We found varied memory effects across different PFTs, with relatively lower antecedent contributions for GRA (average rooting depth 2.5 m), SAV (6.9 m), and WSA (6.2 m) compared to EBF (9.7 m). For example, 74% of the precipitation contribution to EF predictions in EBF arises from antecedent precipitation, followed by 64% in WSA, 65% in

https://doi.org/10.5194/egusphere-2025-4082
Preprint. Discussion started: 29 August 2025

SAV, and 59% in GRA (Figure 8). Notably, for the forest sites, precipitation from almost six months earlier still accounted for 29% ($\sum_{-365}^{-175} EG$) of the EF predictions (Figure 8). However, it is important to note that memory effects vary substantially within most classes, while land-cover classifications only crudely capture the heterogeneous responses of vegetation to water stress (Konings and Gentine, 2017). Further investigation is needed to better elucidate the relationships across diverse PFTs.

The maximum duration of the precipitation reveals that the legacy effect of winter precipitation, occurring 365 days prior, continues to impact water use strategies, as shown by our analysis. This observation aligns with the previous studies and experimental findings. For instance, antecedent winter precipitation from one or two years prior has been shown to influence growth in the current period (Bose et al., 2024; Kannenberg et al., 2020; Marqués et al., 2022; Shen et al., 2016). While legacy effects have been widely reported for winter precipitation in temperate ecosystems, similar effects may also result from summer precipitation in regions where it dominates annual rainfall (e.g., tropical zones or monsoonal regions). Further investigation at the seasonal and event scale is warranted to differentiate the contributions of summer versus winter precipitation memory. The contributions of the memory effect can also be observed for other variables, such as VPD, air temperature and radiation. This indicates the different rooting depths and plant water use strategies that regulate the time scales of droughts, which deserved to be further investigated. Therefore, we emphasize that ignoring the memory effect or legacy effect can introduce bias in detecting the main drivers and hinder a comprehensive understanding of key processes. Our framework provides event-level insights that can be leveraged to explore seasonal variations in ecosystem memory and the co-regulation of EF by multiple climate drivers. These insights lay the groundwork for future classification and clustering analyses aimed at characterizing diverse memory regimes across different climate contexts.

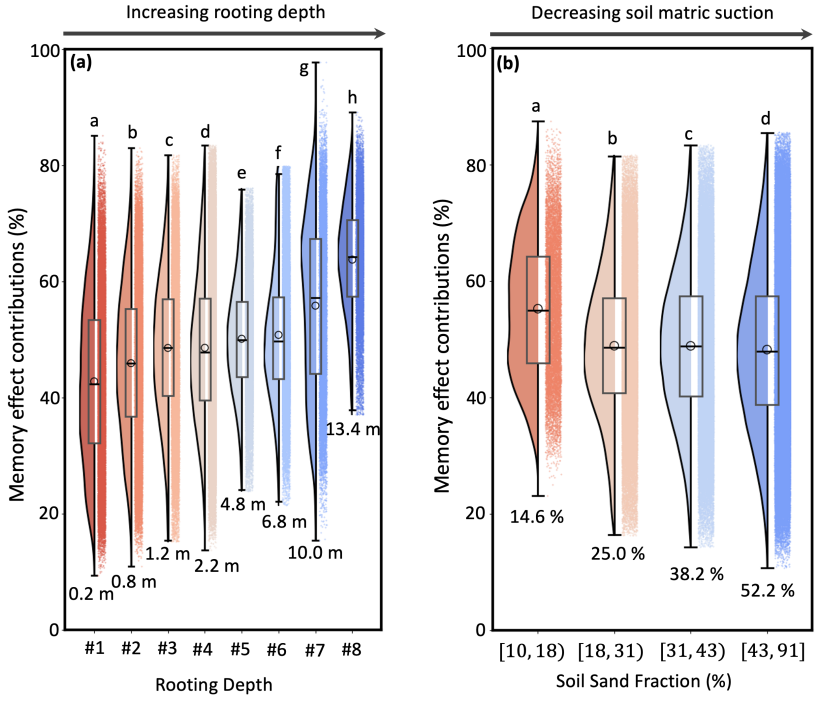

https://doi.org/10.5194/egusphere-2025-4082
Preprint. Discussion started: 29 August 2025

Figure 9. The Relationship Between Rooting Depth, Soil Water Holding Capacity, and the Memory Effect as Captured by the Temporal Memory-Aware Model. The relationship between memory effect contributions to Evaporative Fraction predictions and the rooting depth (a), soil sand fraction (b). Memory effect is defined as the sum of expected gradients (EG) for antecedent periods, this is, $\sum_{-365}^{-7} \boldsymbol{EG}$ represents the sum of absolute EGs between previous 7 and 365 days, for precipitation. The sum absolute EGs are further normalized to a relative percent contribution compared to the concurrent effect ($\sum_{-7}^{0} \boldsymbol{EG}$) for each EF predictions. In the box plots, the central lines represent the median values, the circle represent the mean values, the upper and lower box limits represent the 75th and 25th percentiles, and the upper and lower whiskers extend to 1.5 times the interquartile range, respectively. The violin plot shows the data points density distributions. Letters denote statistically significant differences in the average memory effect contributions values (Tukey's HSD test, P<0.05). Higher soil sand fractions correspond to lower soil matric suction. Deeper rooting depth enables plants to access more water stored from the previous wet season (as illustrated in Figure 1(a)). Data sources include soil sand fraction data from SoilGrid (Poggio et al., 2021) and rooting depth data from Stocker et al., 2023.

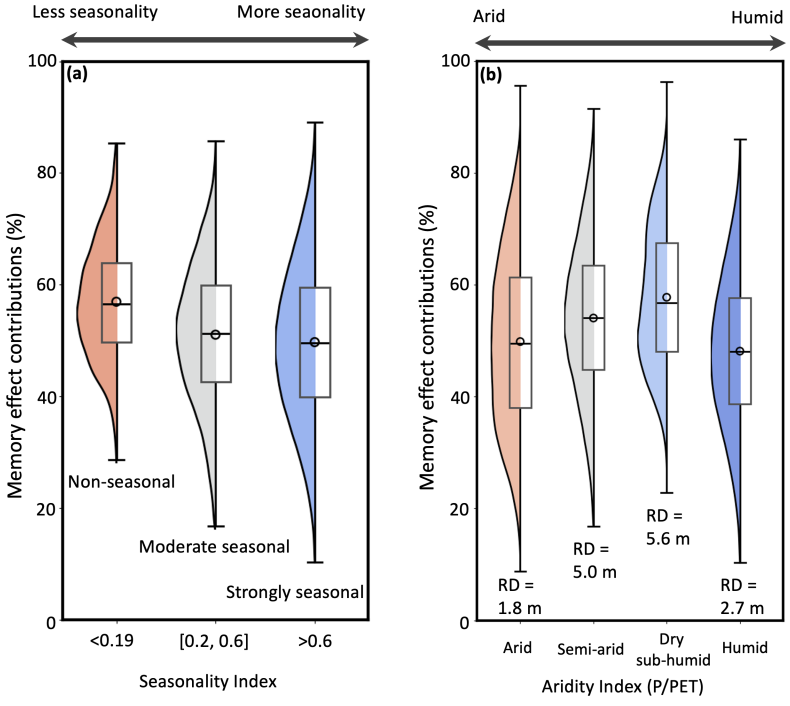

Figure 10. The Relationship Between Seasonality index, Aridity Index, and the Memory Effect as Captured by the Temporal Memory-Aware Model. The relationship between memory effect contributions to Evaporative Fraction predictions and the seasonality index (a), aridity index (b). In the box plots, the central lines represent the median values, the circle represent the mean values, the upper and lower box limits represent the 75th and 25th percentiles, and the upper and lower whiskers extend to 1.5 times the interquartile range, respectively. The violin plot shows the data points density distributions. The annual mean ratio of precipitation to potential evapotranspiration is used as an aridity index. Data sources include TerraClimate (for the aridity index calculation) via Google Earth Engine (Abatzoglou et al., 2018).

We further explored the hidden information within the memory effect by examining its relationship with soil sand fraction (an indicator of soil matric suction and soil water holding capacity), rooting depth, seasonality index and the aridity index across different PFTs. The results underscore the importance of the memory effect captured by our model in reflecting

https://doi.org/10.5194/egusphere-2025-4082
Preprint. Discussion started: 29 August 2025

diverse plant water use strategies, as initially motivated in Figure 1 to use fast and slow EF decay rates to infer plant water use strategies. Our findings reveal that the memory effect increases with deeper plant rooting depths. Vegetation with deep roots, such as forests, can access deep soil water storage derived from precipitation during antecedent periods, resulting in a stronger memory effect (averaging up to 65% contribution). Conversely, vegetation with shallow roots relies more on soil water stored in recent periods, showing a weaker memory effect (45% contribution on average). These results highlight the potential of EF dynamics to serve as indicators of plant water stress and water use strategies. Additionally, plant-available water storage is influenced not only by rooting depth but also by soil water holding capacity (Piedallu et al., 2011). When we examined the relationship between memory effect and soil sand fraction, we found that higher soil sand fractions corresponding to a decreasing memory effect due to reduced soil suction, which limits the soil's ability to retain precipitation from antecedent periods. In the field experiments, sandy soil was found to hold significantly less plant-available water per foot of soil compared to silt loam (Shwetha and Varija, 2015; Verheijen et al., 2019). While there is a general monotonic decrease in the memory effect with increasing soil sand fraction, rooting depth remains a critical factor, with both factors jointly regulating plant water use strategies (Figure 9(b)). In line with this, previous studies demonstrated that vegetation functioning during drought years in the Amazon rainforest is shaped by both rooting depth and water table depth (WTD). Thus, incorporating reliable WTD datasets into future analyses could provide deeper insight into subsurface water access and its role in modulating vegetation responses and memory effects.

In addition, we found that memory effect contributions generally decrease with increasing seasonality index (SI) (Figure 10). This suggests that ecosystems in highly seasonal climates tend to rely more on short-term rain pulses and instantaneous climatic drivers rather than antecedent conditions. One possible explanation is that sharp dry-wet seasonal transitions shorten biologically active periods, thereby limiting the time window over which memory effects can persist. However, it is important to note that memory is often co-regulated by multiple climatic drivers, such as precipitation and temperature, and their interactions may vary across ecosystems. Therefore, further investigation is needed to fully understand the underlying mechanisms and to disentangle the role of seasonality in regulating memory effects.

In dry areas, such as woody savannas, savannas, and open shrublands, shallow rooting depths and high soil sand fractions (e.g., in deserts or the Gobi region) result in lower memory effect contributions (49% on average for aridity indices below 0.2). In wetter areas, forests with deeper rooting depths and lower soil sand fractions are better equipped to utilize water stored from antecedent precipitation, resulting in higher memory effects (59% on average). Notably, rooting depth exerts a dominant control even in humid ecosystems, underscoring its overarching role in shaping memory effects (Figure 10b). Our analysis suggests that the memory effect holds potential as a proxy for rooting depth - a factor that are often difficult to measure and have been largely overlooked in many studies and Earth system models. However, further investigation is still required to fully understand the complex mechanisms governing the interaction between these factors. Neglecting the memory effect could lead to a reduced understanding of the water, energy and carbon cycle, limiting our ability to model and predict these critical processes accurately.

https://doi.org/10.5194/egusphere-2025-4082
Preprint. Discussion started: 29 August 2025

5 Conclusions

In this study, we developed an explainable machine learning model that incorporates the memory effects of meteorological drivers to better understand the mechanisms controlling evaporative fraction—a key indicator of plant water stress. The model was trained using eddy covariance data from the combined ICOS, AmeriFlux, and FLUXNET2015 Tier 1 datasets. Our main findings are as follows:

1) The LSTM model demonstrated strong performance across diverse plant functional types, outperforming all baseline models on test datasets.
2) The model adequately captures and reconstructs the EF dynamics, particularly during soil moisture dry-down periods very well and these observations are consistent with soil moisture decay patterns.
3) By accounting for the memory effect, air temperature and precipitation rather than radiation, emerged as the most influential driver of EF predictions, followed by VPD. Notably, the expected gradients' temporal analysis indicated that the model accounts for more historical time steps for forest and savanna sites compared to grassland sites, likely due to differences in vegetation rooting depths and water usage strategies. Our analysis suggests grassland sites generally rely on shorter time periods, spanning several months, for most of EF predictions.
4) Further investigation reveals that memory effect is closely associated with rooting depth, soil sand fractions, seasonality index, and aridity index. These findings highlight novel mechanisms that emerge only when the memory effect is considered. This underscores the potential of using the EF across diverse PFTs to reflect varying plant water stress conditions and water use strategies.

Our results highlight the critical importance of the memory effect in EF predictions and carry significant implications for assessing ecosystem water stress and predicting it months in advance. For instance, water shortages from the previous year can still impact ecosystem functioning in the current year, particularly in forests. Incorporating this memory-awareness into our modeling approach opens new opportunities to infer varying rooting depth across biomes from surface measurements – an important yet often overlooked factor in land surface and earth system modeling.

Acknowledgments

P.G. and W.Z. would like to acknowledge funding from the Land Ecosystem Models based On New Theory, obseRvations and ExperimEnts (LEMONTREE) project, and National Science Foundation Science and Technology Center LEAP, Learning the Earth with Artificial intelligence and Physics, as well as support from NASA grant 80NSSC18K0998. A.J.W., P.G. and W.Z., M.R. acknowledge support by the European Research Council (ERC) Synergy Grant "Understanding and Modelling the Earth System with Machine Learning (USMILE)" under the Horizon 2020 research and innovation program (Grant agreement No.855187). W.Z. would like to acknowledge the scholarship awarded by the Max Planck Institute for Biogeochemistry. We extend our sincere thanks to Dr. Christian Reimers from the Max Planck Institute for Biogeochemistry for reviewing and improving the readability of the entire manuscript. We acknowledge the data resources provided by the

https://doi.org/10.5194/egusphere-2025-4082
Preprint. Discussion started: 29 August 2025

Integrated Carbon Observation System (ICOS), AmeriFlux, and FLUXNET2015 Tier 1. The AmeriFlux data were supported by the U.S. Department of Energy's Office of Science. The FLUXNET2015 Tier 1 dataset was produced by the FLUXNET community and data-contributing networks (including AmeriFlux, AsiaFlux, CarboEurope, ICOS, OzFlux, and others), with support from the U.S. Department of Energy, the European Union's Horizon 2020 research and innovation programme, and other funding agencies.

Author contributions

W. Z., A.J. W., and P. G. designed the study. W.Z. performed the analyses, with additional support from Ulrich Weber on datasets preprocessing. W.Z. led the writing with input from all co-authors.

Competing financial interests

The authors declare that they have no conflict of interest.

References

Abatzoglou, J. T., Dobrowski, S. Z., Parks, S. A., and Hegewisch, K. C.: TerraClimate, a high-resolution global dataset of monthly climate and climatic water balance from 1958–2015, Sci Data, 5, 170191, https://doi.org/10.1038/sdata.2017.191, 2018.

Bastiaanssen, W. G. M., Pelgrum, H., Droogers, P., De Bruin, H. A. R., and Menenti, M.: Area-average estimates of evaporation, wetness indicators and top soil moisture during two golden days in EFEDA, Agricultural and Forest Meteorology, 87, 119–137, https://doi.org/10.1016/S0168-1923(97)00020-8, 1997.

Bose, A. K., Doležal, J., Scherrer, D., Altman, J., Ziche, D., Martínez-Sancho, E., Bigler, C., Bolte, A., Colangelo, M., Dorado-Liñán, I., Drobyshev, I., Etzold, S., Fonti, P., Gessler, A., Kolář, T., Koňasová, E., Korznikov, K. A., Lebourgeois, F., Lucas-Borja, M. E., Menzel, A., Neuwirth, B., Nicolas, M., Omelko, A. M., Pederson, N., Petritan, A. M., Rigling, A., Rybníček, M., Scharnweber, T., Schröder, J., Silla, F., Sochová, I., Sohar, K., Ukhvatkina, O. N., Vozmishcheva, A. S., Zweifel, R., and Camarero, J. J.: Revealing legacy effects of extreme droughts on tree growth of oaks across the Northern Hemisphere, Science of The Total Environment, 926, 172049, https://doi.org/10.1016/j.scitotenv.2024.172049, 2024.

Chen, Y., Xue, Y., and Hu, Y.: How multiple factors control evapotranspiration in North America evergreen needleleaf forests, Science of The Total Environment, 622–623, 1217–1224, https://doi.org/10.1016/j.scitotenv.2017.12.038, 2018.

Collins, D. B. G. and Bras, R. L.: Plant rooting strategies in water-limited ecosystems, Water Resources Research, 43, 2006WR005541, https://doi.org/10.1029/2006WR005541, 2007.

Dralle, D. N., Jesse Hahm, W., Rempe, D. M., Karst, N., Anderegg, L. D. L., Thompson, S. E., Dawson, T. E., and Dietrich, W. E.: Plants as sensors: vegetation response to rainfall predicts root-zone water storage capacity in Mediterranean-type climates, Environ. Res. Lett., 15, 104074, https://doi.org/10.1088/1748-9326/abb10b, 2020.

https://doi.org/10.5194/egusphere-2025-4082
Preprint. Discussion started: 29 August 2025

ElGhawi, R., Kraft, B., Reimers, C., Reichstein, M., Körner, M., Gentine, P., and Winkler, A. J.: Hybrid modeling of evapotranspiration: inferring stomatal and aerodynamic resistances using combined physics-based and machine learning, Environ. Res. Lett., 18, 034039, https://doi.org/10.1088/1748-9326/acbbe0, 2023.

Erion, G., Janizek, J. D., Sturmfels, P., Lundberg, S. M., and Lee, S.-I.: Improving performance of deep learning models with axiomatic attribution priors and expected gradients, Nat Mach Intell, 3, 620–631, https://doi.org/10.1038/s42256-021-00343-w, 2021.

Fan, Y., Miguez-Macho, G., Jobbágy, E. G., Jackson, R. B., and Otero-Casal, C.: Hydrologic regulation of plant rooting depth, Proc. Natl. Acad. Sci. U.S.A., 114, 10572–10577, https://doi.org/10.1073/pnas.1712381114, 2017.

Fang, K. and Shen, C.: Near-real-time forecast of satellite-based soil moisture using long short-term memory with an adaptive data integration kernel, Journal of Hydrometeorology, 21, 399–413, 2020.

Feng, D., Fang, K., and Shen, C.: Enhancing Streamflow Forecast and Extracting Insights Using Long-Short Term Memory Networks With Data Integration at Continental Scales, Water Resources Research, 56, e2019WR026793, https://doi.org/10.1029/2019WR026793, 2020.

Foken, T.: The energy balance closure problem: An overview, Ecological Applications, 18, 1351–1367, 2008.

Fu, Z., Ciais, P., Makowski, D., Bastos, A., Stoy, P. C., Ibrom, A., Knohl, A., Migliavacca, M., Cuntz, M., Šigut, L., Peichl, M., Loustau, D., El-Madany, T. S., Buchmann, N., Gharun, M., Janssens, I., Markwitz, C., Grünwald, T., Rebmann, C., Mölder, M., Varlagin, A., Mammarella, I., Kolari, P., Bernhofer, C., Heliasz, M., Vincke, C., Pitacco, A., Cremonese, E., Foltýnová, L., and Wigneron, J.: Uncovering the critical soil moisture thresholds of plant water stress for European ecosystems, Global Change Biology, 28, 2111–2123, https://doi.org/10.1111/gcb.16050, 2022.

Fu, Z., Ciais, P., Wigneron, J.-P., Gentine, P., Feldman, A. F., Makowski, D., Viovy, N., Kemanian, A. R., Goll, D. S., Stoy, P. C., Prentice, I. C., Yakir, D., Liu, L., Ma, H., Li, X., Huang, Y., Yu, K., Zhu, P., Li, X., Zhu, Z., Lian, J., and Smith, W. K.: Global critical soil moisture thresholds of plant water stress, Nat Commun, 15, 4826, https://doi.org/10.1038/s41467-024-49244-7, 2024.

Gentine, P., Entekhabi, D., Chehbouni, A., Boulet, G., and Duchemin, B.: Analysis of evaporative fraction diurnal behaviour, Agricultural and Forest Meteorology, 143, 13–29, https://doi.org/10.1016/j.agrformet.2006.11.002, 2007.

Gentine, P., Entekhabi, D., and Polcher, J.: The Diurnal Behavior of Evaporative Fraction in the Soil–Vegetation–Atmospheric Boundary Layer Continuum, Journal of Hydrometeorology, 12, 1530–1546, https://doi.org/10.1175/2011JHM1261.1, 2011.

Guérin, M., Von Arx, G., Martin-Benito, D., Andreu-Hayles, L., Griffin, K. L., McDowell, N. G., Pockman, W., and Gentine, P.: Distinct xylem responses to acute vs prolonged drought in pine trees, Tree Physiology, 40, 605–620, https://doi.org/10.1093/treephys/tpz144, 2020.

Hollinger, D. and Richardson, A.: Uncertainty in eddy covariance measurements and its application to physiological models, Tree physiology, 25, 873–885, 2005.

Ichii, K., Wang, W., Hashimoto, H., Yang, F., Votava, P., Michaelis, A. R., and Nemani, R. R.: Refinement of rooting depths using satellite-based evapotranspiration seasonality for ecosystem modeling in California, Agricultural and Forest Meteorology, 149, 1907–1918, https://doi.org/10.1016/j.agrformet.2009.06.019, 2009.

https://doi.org/10.5194/egusphere-2025-4082
Preprint. Discussion started: 29 August 2025

Jiang, S., Zheng, Y., and Solomatine, D.: Improving AI System Awareness of Geoscience Knowledge: Symbiotic Integration of Physical Approaches and Deep Learning, Geophys Res Lett, 47, https://doi.org/10.1029/2020GL088229, 2020.

Jiang, S., Bevacqua, E., and Zscheischler, J.: River flooding mechanisms and their changes in Europe revealed by explainable machine learning, Hydrol Earth Syst Sc, 26, 6339–6359, https://doi.org/10.5194/hess-26-6339-2022, 2022a.

Jiang, S., Zheng, Y., Wang, C., and Babovic, V.: Uncovering Flooding Mechanisms Across the Contiguous United States Through Interpretive Deep Learning on Representative Catchments, Water Resources Research, 58, e2021WR030185, https://doi.org/10.1029/2021WR030185, 2022b.

Kannenberg, S. A., Schwalm, C. R., and Anderegg, W. R. L.: Ghosts of the past: how drought legacy effects shape forest functioning and carbon cycling, Ecology Letters, 23, 891–901, https://doi.org/10.1111/ele.13485, 2020.

Konings, A. G. and Gentine, P.: Global variations in ecosystem-scale isohydricity, Global Change Biology, 23, 891–905, https://doi.org/10.1111/gcb.13389, 2017.

Kraft, B., Jung, M., Körner, M., Requena Mesa, C., Cortés, J., and Reichstein, M.: Identifying Dynamic Memory Effects on Vegetation State Using Recurrent Neural Networks, Front. Big Data, 2, 31, https://doi.org/10.3389/fdata.2019.00031, 2019.

Kraft, B., Jung, M., Körner, M., Koirala, S., and Reichstein, M.: Towards hybrid modeling of the global hydrological cycle, Hydrol. Earth Syst. Sci., 26, 1579–1614, https://doi.org/10.5194/hess-26-1579-2022, 2022.

Lees, T., Reece, S., Kratzert, F., Klotz, D., Gauch, M., De Bruijn, J., Kumar Sahu, R., Greve, P., Slater, L., and Dadson, S.: Hydrological concept formation inside long short-term memory (LSTM) networks, Hydrology and Earth System Sciences Discussions, 2021, 1–37, 2021.

Lees, T., Reece, S., Kratzert, F., Klotz, D., Gauch, M., De Bruijn, J., Kumar Sahu, R., Greve, P., Slater, L., and Dadson, S. J.: Hydrological concept formation inside long short-term memory (LSTM) networks, Hydrol. Earth Syst. Sci., 26, 3079–3101, https://doi.org/10.5194/hess-26-3079-2022, 2022.

Lhomme, J.-P. and Elguero, E.: Examination of evaporative fraction diurnal behaviour using a soil-vegetation model coupled with a mixed-layer model, Hydrology and Earth System Sciences, 3, 259–270, 1999.

Li, Q., Zhu, Y., Shangguan, W., Wang, X., Li, L., and Yu, F.: An attention-aware LSTM model for soil moisture and soil temperature prediction, Geoderma, 409, 115651, https://doi.org/10.1016/j.geoderma.2021.115651, 2022.

Lian, X., Zhao, W., and Gentine, P.: Recent global decline in rainfall interception loss due to altered rainfall regimes, Nat Commun, 13, 7642, https://doi.org/10.1038/s41467-022-35414-y, 2022.

Liu, X., Chen, F., Barlage, M., and Niyogi, D.: Implementing Dynamic Rooting Depth for Improved Simulation of Soil Moisture and Land Surface Feedbacks in Noah-MP-Crop, J Adv Model Earth Sy, 12, https://doi.org/10.1029/2019MS001786, 2020.

Loveland, T. R., Reed, B. C., Brown, J. F., Ohlen, D. O., Zhu, Z., Yang, L., and Merchant, J. W.: Development of a global land cover characteristics database and IGBP DISCover from 1 km AVHRR data, International journal of remote sensing, 21, 1303–1330, 2000.

Marqués, L., Peltier, D. M. P., Camarero, J. J., Zavala, M. A., Madrigal-González, J., Sangüesa-Barreda, G., and Ogle, K.: Disentangling the Legacies of Climate and Management on Tree Growth, Ecosystems, 25, 215–235, https://doi.org/10.1007/s10021-021-00650-8, 2022.

https://doi.org/10.5194/egusphere-2025-4082
Preprint. Discussion started: 29 August 2025

McColl, K. A., Wang, W., Peng, B., Akbar, R., Short Gianotti, D. J., Lu, H., Pan, M., and Entekhabi, D.: Global characterization of surface soil moisture drydowns, Geophys. Res. Lett., 44, 3682–3690, https://doi.org/10.1002/2017GL072819, 2017.

Molnar, C.: Interpretable machine learning, 2019.

Nutini, F., Boschetti, M., Candiani, G., Bocchi, S., and Brivio, P.: Evaporative Fraction as an Indicator of Moisture Condition and Water Stress Status in Semi-Arid Rangeland Ecosystems, Remote Sensing, 6, 6300–6323, https://doi.org/10.3390/rs6076300, 2014.

Pan, S., Pan, N., Tian, H., Friedlingstein, P., Sitch, S., Shi, H., Arora, V. K., Haverd, V., Jain, A. K., and Kato, E.: Evaluation of global terrestrial evapotranspiration using state-of-the-art approaches in remote sensing, machine learning and land surface modeling, Hydrology and Earth System Sciences, 24, 1485–1509, 2020.

Piedallu, C., Gégout, J.-C., Bruand, A., and Seynave, I.: Mapping soil water holding capacity over large areas to predict potential production of forest stands, Geoderma, 160, 355–366, https://doi.org/10.1016/j.geoderma.2010.10.004, 2011.

Poggio, L., de Sousa, L. M., Batjes, N. H., Heuvelink, G. B. M., Kempen, B., Ribeiro, E., and Rossiter, D.: SoilGrids 2.0: producing soil information for the globe with quantified spatial uncertainty, SOIL, 7, 217–240, https://doi.org/10.5194/soil-7-217-2021, 2021.

Reichstein, M., Camps-Valls, G., Stevens, B., Jung, M., Denzler, J., Carvalhais, N., and Prabhat, fnm: Deep learning and process understanding for data-driven Earth system science, Nature, 566, 195–204, 2019.

Reichstein, M., Ahrens, B., Kraft, B., Camps-Valls, G., Carvalhais, N., Gans, F., Gentine, P., and Winkler, A. J.: Combining system modeling and machine learning into hybrid ecosystem modeling, in: Knowledge Guided Machine Learning, Chapman and Hall/CRC, 327–352, 2022.

Richardson, A. D., Hollinger, D. Y., Burba, G. G., Davis, K. J., Flanagan, L. B., Katul, G. G., Munger, J. W., Ricciuto, D. M., Stoy, P. C., and Suyker, A. E.: A multi-site analysis of random error in tower-based measurements of carbon and energy fluxes, Agricultural and Forest Meteorology, 136, 1–18, 2006.

Schwalm, C. R., Williams, C. A., Schaefer, K., Arneth, A., Bonal, D., Buchmann, N., Chen, J., Law, B. E., Lindroth, A., Luyssaert, S., Reichstein, M., and Richardson, A. D.: Assimilation exceeds respiration sensitivity to drought: A FLUXNET synthesis, Global Change Biology, 16, 657–670, https://doi.org/10.1111/j.1365-2486.2009.01991.x, 2010.

Seyfried, M. S. and Wilcox, B. P.: Soil water storage and rooting depth: key factors controlling recharge on rangelands, Hydrological Processes, 20, 3261–3275, https://doi.org/10.1002/hyp.6331, 2006.

Shen, W., Jenerette, G. D., Hui, D., and Scott, R. L.: Precipitation legacy effects on dryland ecosystem carbon fluxes: direction, magnitude and biogeochemical carryovers, Biogeosciences, 13, 425–439, https://doi.org/10.5194/bg-13-425-2016, 2016.

Shwetha, P. and Varija, K.: Soil Water Retention Curve from Saturated Hydraulic Conductivity for Sandy Loam and Loamy Sand Textured Soils, Aquatic Procedia, 4, 1142–1149, https://doi.org/10.1016/j.aqpro.2015.02.145, 2015.

Staacke, T., Mueller-Roeber, B., and Balazadeh, S.: Stress resilience in plants: the complex interplay between heat stress memory and resetting, New Phytologist, 245, 2402–2421, https://doi.org/10.1111/nph.20377, 2025.

https://doi.org/10.5194/egusphere-2025-4082
Preprint. Discussion started: 29 August 2025

Stocker, B. D., Tumber-Dávila, S. J., Konings, A. G., Anderson, M. C., Hain, C., and Jackson, R. B.: Global patterns of water storage in the rooting zones of vegetation, Nat. Geosci., https://doi.org/10.1038/s41561-023-01125-2, 2023.

Sundararajan, M., Taly, A., and Yan, Q.: Axiomatic Attribution for Deep Networks, http://arxiv.org/abs/1703.01365, 12 June 2017.

Verheijen, F. G. A., Zhuravel, A., Silva, F. C., Amaro, A., Ben-Hur, M., and Keizer, J. J.: The influence of biochar particle size and concentration on bulk density and maximum water holding capacity of sandy vs sandy loam soil in a column experiment, Geoderma, 347, 194–202, https://doi.org/10.1016/j.geoderma.2019.03.044, 2019.

Wang, K., Li, Z., and Cribb, M.: Estimation of evaporative fraction from a combination of day and night land surface temperatures and NDVI: A new method to determine the Priestley–Taylor parameter, Remote Sensing of Environment, 102, 293–305, https://doi.org/10.1016/j.rse.2006.02.007, 2006.

Williams, I. N. and Torn, M. S.: Vegetation controls on surface heat flux partitioning, and land-atmosphere coupling, Geophysical Research Letters, 42, 9416–9424, https://doi.org/10.1002/2015GL066305, 2015.

Xiao, L., Wu, X., Zhao, S., and Zhou, J.: Memory effects of vegetation after extreme weather events under various geological conditions in a typical karst watershed in southwestern China, Agricultural and Forest Meteorology, 345, 109840, https://doi.org/10.1016/j.agrformet.2023.109840, 2024.

Yang, W., Shabanov, N., Huang, D., Wang, W., Dickinson, R., Nemani, R., Knyazikhin, Y., and Myneni, R.: Analysis of leaf area index products from combination of MODIS Terra and Aqua data, Remote Sensing of Environment, 104, 297–312, 2006.

Zenone, T., Vitale, L., Famulari, D., and Magliulo, V.: Application of machine learning techniques to simulate the evaporative fraction and its relationship with environmental variables in corn crops, Ecol Process, 11, 54, https://doi.org/10.1186/s13717-022-00400-1, 2022.

Zhang, Y., Keenan, T. F., and Zhou, S.: Exacerbated drought impacts on global ecosystems due to structural overshoot, Nat Ecol Evol, 5, 1490–1498, https://doi.org/10.1038/s41559-021-01551-8, 2021.

Zhao, W. L., Gentine, P., Reichstein, M., Zhang, Y., Zhou, S., Wen, Y., Lin, C., Li, X., and Qiu, G. Y.: Physics-Constrained Machine Learning of Evapotranspiration, Geophysical Research Letters, 46, 14496–14507, https://doi.org/10.1029/2019GL085291, 2019.